Wind Tunnel Test of Trailing Edge Serrations for the Reduction of Wind Turbine Noise

Andreas FISCHER[1]; Franck BERTAGNOLIO[1]; Wen Zhong SHEN[1]; Jesper MADSEN[3] ; Helge Aagaard MADSEN[1]; Christian BAK[1]; William DEVENPORT[2]; Nanyaporn INTARATEP[2]

[1] Technical University of Denmark (DTU), Denmark

[2] Virginia Tech University, USA

[3] LM Wind Power A/S, Denmark

ABSTRACT

We tested trailing edge serrations for the reduction of the emitted sound from an aerofoil in the aero-acoustic wind tunnel of Virginia Tech University. The aerofoil was developed for the use on the outer part of the blade of a wind turbine. Two different serration geometries were tested. The geometry of the serrations is confidential to LM Wind Power A/S. The far field sound was measured with a microphone array outside the test section. Additionally the aerofoil surface pressure was measured at 62 chordwise positions. The chord based Reynolds number was 1.6 million. The serrations had very small influence on the aerodynamic performance of the aerofoil. At low angles the emitted sound was decreased by up to 8 dB, but the noise reduction became less with increasing angle of attack. At very high angles of attack the emitted sound was increased. The measured far field sound was compared to a modified TNO model using Howe's expression for sound emitted from a serrated edge. The comparison was good for the straight edge configuration, but the noise reduction by a serrated edge was significantly overestimated by the model. The expression for sinusoidal serrations gave better results than the one for saw-tooth serrations.

Keywords: trailing edge serrations, noise reduction, wind tunnel test

1. INTRODUCTION

Public annoyance due to experienced or perceived noise from wind turbine is a significant barrier for development of wind energy on land. Wind energy from land-based wind farms has a significantly lower cost of energy than offshore while being comparable in cost with new gas-fired power plants at good wind sites. On land the primary issue is aerodynamic noise. Decreasing the aerodynamic noise will increase the public acceptance of wind energy and accelerate of onshore wind energy. Trailing edge (TE) serrations have shown to reduce noise from wind turbines significantly (1).

Even though the noise reduction potential of TE serrations for aerofoil sections (2) and wind turbines is experimentally well documented, the mechanisms behind the noise reduction are not fully understood. More research is needed to exploit the full noise reduction potential of serrations on wind turbines. Therefore an experiment in the aero acoustic wind tunnel of Virginia Tech was conducted. The aerodynamic performance and the far field sound pressure emitted from an aerofoil developed for wind turbine blades were measured simultaneously. Two different types of serrations were tested on the aerofoil.

An semi-empirical model for TE noise predictions (3) was modified to include the effect of a serrated TE (4, 5). The results of the model were compared to measurements to get new insight in the way how serrations work.

The paper is organised in the following way. First the experimental set-up and the wind tunnel are described. Then the analytical solutions to describe the diffraction of the surface pressure passing by a serrated TE (4, 5) are outlined and discussed. Next, the results of the study are presented. This section is divided into the analysis of the aerodynamic performance of the aerofoil with and without serrations, followed by the analysis of the far field sound pressure measurements for the different configurations and rounded up by the comparison of the far field sound measurements with computations. The paper is concluded by a summary of the most important results.

[1] asfi@dtu.dk

2. EXPERIMENTAL SET-UP

2.1 The Virginia Tech Stability Wind Tunnel

The Virginia Tech Stability Wind Tunnel (VTST)(6) is a closed loop subsonic wind tunnel with a 1.83 m x 1.83 m rectangular removable test section. The length of the test section is 7.3 m. A flow speed of 75 m/s can be reached with an empty test section. An air exchange tower open to the atmosphere is located downstream of the fan. Turbulence intensities of less than 0.05% were reported from measurements in the aerodynamic test section.

In the present experiment an acoustic test section with Kevlar walls was used. The acoustic test section is surrounded by anechoic chambers. The Kevlar walls were designed to contain the flow and keep the same aerodynamic performance as with a closed test section while sound waves are transmitted through the walls and can be measured in the anechoic chamber. The anechoic limit of the acoustic configuration is 190 Hz.

The aerodynamic wind tunnel data was corrected for the influence of the Kevlar walls by a panel method (6). The method takes into account the deflection of the Kevlar walls under load, the development of the boundary layer on the deflected walls and the transpiration of air through the Kevlar walls. The corrected aerodynamic data presented in this paper corresponds to conditions of an unbounded flow field. The advantage of the Kevlar walled acoustic test section compared to traditional open jet acoustic wind tunnel is that the magnitude of the aerodynamic corrections is much smaller.

The static pressure and the flow temperature in the test section are monitored during the experiment. The flow speed in the test section is determined by a measurement of the pressure in the settling chamber and downstream of the contraction. The contraction and settling chamber pressure are measured with an Esterline 9816/98RK pressure scanner with a range of $\pm$2.5 psi. The system has a rated accuracy of $\pm$0.05% of the full scale. The mean pressure distribution on the aerofoil was also recorded with the Esterline pressure scanner.

A microphone array consisting of 117 microphones was located in the starboard anechoic chamber. The microphones were arranged in a 9-armed spiral of 13 microphones. The diameter of the array disc is 1.1 m. The position of the microphone array relative to the aerofoil is shown in figure 1. The microphones used in

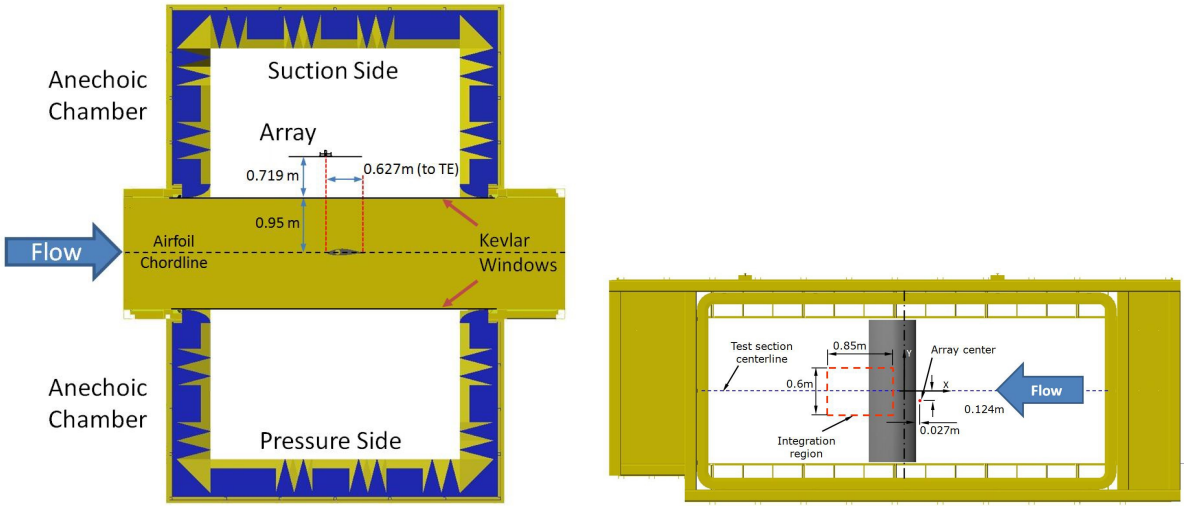

(a) top view (b) starboard view

Figure 1 – The wind tunnel test section, the aerofoil and the microphone array.

this array are Panasonic model WM-64PNT Electret microphones. These microphones have a flat frequency response from 20-16000 Hz and a sensitivity of -44$\pm$3 dB Re 1 V/Pa at 1 kHz. All microphones used in the array were calibrated before being installed in the array and selected to be within $\pm5^\circ$ phase and $\pm$0.4 dB amplitude from 500 Hz to 16000 Hz.

2.2 Processing of the microphone array data

The microphone data were sampled with a 128-channel data acquisition system with a maximum sampling frequency of 200 kHz. A signal conditioning and filtering box designed by AVEC provided a low pass filter with a corner frequency of 20 kHz to avoid aliasing. The conditioned signals were fed to a computer with two 64-channel PCI-based data acquisition cards. The data were processed with frequency domain beamforming to extract the sound pressure level of the TE source from the background noise. The time series were measured with a sampling frequency of 51200 Hz during a period of 32 seconds. It was divided into 200 blocks of 8192

samples to compute the averaged cross spectral density matrix. The beamforming algorithm proposed by (7) was used, which is different compared to classical beamforming in two points:

- The diagonal of the cross spectral density matrix is removed
- The refraction of the sound waves penetrating the boundary layer at the Kevlar wall is accounted for by a ray tracing method

To improve the beamforming maps the microphone array was carefully calibrated after installation.
The beamforming maps are integrated to obtain the far field sound pressure spectrum. The integration area was chosen to allow a separation of the TE source from spurious noise caused by the aerofoil/wind tunnel junction. It extends 0.6 m of the aerofoil span and its position is shown in figure 1(b).
The integrated sound pressure spectrum was corrected for losses due to the transmission of sound through the Kevlar windows and the boundary layer built up on the Kevlar wall. The correction for both effects is a frequency dependent factor given in (6). The beamforming maps were not corrected for the transmission losses.

2.3 Wind tunnel model and serrations

The model used in the experiment was a LN118 aerofoil, fig. 2. The aerofoil shape was developed for the

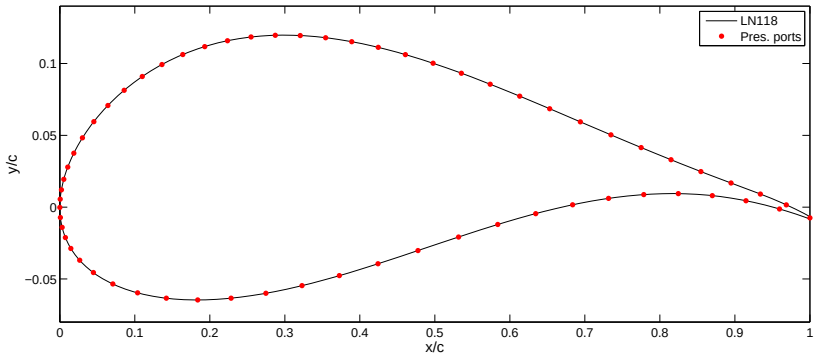

Figure 2 – The LN118 aerofoil and the pressure port location

use at the outer blade sections of a wind turbine (8). The design goals were high aerodynamic performance and minimised emission of TE noise. The noise constraint led to the very high curvature and characteristic shape in the TE region.
The aerofoil model had a chord length of 0.6 m and a span of 1.82 m. The TE thickness was 1.0 mm. The average roughness of the surface of the model was $R_a = 0.54\ \mu$m. The aerofoil is flush mounted with the wind tunnel walls. It was sealed at the wind tunnel walls with a transition piece made of Urethane foam. The surface of the transition piece in contact with the wind tunnel walls was made of Teflon. At the junction of aerofoil and tunnel walls a approx. 15 mm long Mylar brush was attached to the TE of the aerofoil to reduce spurious noise from the junction of aerofoil and wind tunnel wall. The spanwise extension of the Mylar brush was 250 mm. It was attached on the pressure side of the aerofoil. The geometric zero angle of attack (AoA) is established with an accuracy of $\pm 0.3°$.
The aerofoil was equipped with 62 pressure ports (0.5 mm pinhole diameter). Their distribution is illustrated in figure 2. The pressure ports were offset in spanwise direction to avoid that upstream holes influence the flow over downstream holes.
Two different types of saw-tooth shaped serrations were tested. The geometry of the serrations is proprietary to LM Wind Power A/S. The serrations were attached on the pressure side of the aerofoil and bent towards the suction side.

3. THEORY OF FAR FIELD SOUND REFRACTED ON A SERRATED TRAILING EDGE

Several theories describe the diffraction of the pressure field convecting past the TE of an aerofoil and relate it to the emitted far field sound. The most important publications on this subject are the generalised theory of Howe (9) and the theory of Amiet (10). Those theories are equivalent in the high frequency range. Howe's theory was extended successively to include the effect of sinusoidal shaped serrations (4) and saw-tooth shaped serrations (5). In the following Howe's approach is outlined.

The far field sound pressure generated by a pressure field convecting past a straight TE (9) is given by

$$S(\omega) = \frac{L}{4\pi R^2} \int_{-\infty}^{\infty} \frac{\omega}{|k_1| c_0} \Phi_p(k_1, 0, \omega)\, dk_1. \tag{1}$$

The observer is located perpendicular to the TE and centred over the wetted span. The extend of the wetted span is L and the distance to the observer is R. Φ_p is the surface pressure frequency wave number spectrum at a position of at least one characteristic wave length upstream of the TE. The formula for the surface pressure frequency wave number spectrum was originally developed by Parchen (11) (the so-called TNO model) and extended by Bertagnolio et al. (3) to include anisotropy of the spectral tensor of the velocity in dependence of the local pressure gradient. It reads

$$\Phi_p(k_1, k_3, \omega) = 4\rho^2 \frac{k_1^2}{k_1^2 + k_3^2} \int_0^{\infty} L_{2a} \left(\frac{dU_1}{dy} \right)^2 \Phi_{22a} \Phi_m e^{-\sqrt{k_1^2 + k_3^2} y} dy. \tag{2}$$

L_{2a} is the vertical length scale of the vertical velocity (the subscript a denotes the anisotropic model) and Φ_{22a} is the energy density spectrum of the vertical velocity. The moving axis spectrum Φ_m describes the deformation of the pressure field during convection. In the original model (11) it assumes a Gaussian shape centred at the convective ridge $\omega - U_c k_1$; U_c is the eddy convection velocity. To simplify we assume a Dirac delta function for the moving axis spectrum

$$\Phi_m(k_1, \omega) = \frac{1}{U_c} \delta \left(\frac{\omega}{U_c} - k_1 \right). \tag{3}$$

Using eq. 3 eq. 1 can be reduced to

$$S(\omega) = \frac{L}{4\pi R^2} \frac{1}{c_0} \Phi_p \left(\frac{\omega}{U_c}, 0 \right). \tag{4}$$

Some test computations showed that the result of eq. 1 and eq. 4 differs by less than 0.2 dB in almost all cases. The sound at the observer position as in eq. 1 produced by turbulent flow passing a sinusoidal serrated TE is given by Howe (4) as

$$\tilde{S}(\omega) = \frac{L}{4\pi R^2} \frac{1}{c_0} \sum_{n=-\infty}^{\infty} \frac{\left(\frac{\omega}{U_c} \right)^2 + k_n^2}{\left(\frac{\omega}{U_c} \right)^2} J_n^2 \left(\frac{\omega h}{U_c} \right) \Phi_p \left(\frac{\omega}{U_c}, k_n \right). \tag{5}$$

where

$$k_n = \frac{2\pi n}{\lambda} \tag{6}$$

is the spanwise discrete wave number and λ is the wave length of the serrations. h is half of the peak-to-peak amplitude of the serrations. J_n is a Bessel function of order n. Note that eq. 5 was multiplied by a factor 2 compared to the original expression, eq. 28 in (4), because it must reduce to the result of the sound produced by a straight TE when the wave length of the serrations becomes very large and the amplitude very small. The ratio of eq. 5 and eq. 4 is

$$\frac{\tilde{S}(\omega)}{S(\omega)} = \sum_{n=-\infty}^{\infty} \frac{\left(\frac{\omega}{U_c} \right)^2 + k_n^2}{\left(\frac{\omega}{U_c} \right)^2} J_n^2 \left(\frac{\omega h}{U_c} \right) \frac{\Phi_p \left(\frac{\omega}{U_c}, k_n \right)}{\Phi_p \left(\frac{\omega}{U_c}, 0 \right)}. \tag{7}$$

For very large wave length λ and very small amplitude h eq. 7 goes towards the limit

$$\lim_{\lambda \to \infty, h \to 0} \frac{\tilde{S}(\omega)}{S(\omega)} = \sum_{n=-\infty}^{\infty} J_n^2(0) = 1. \tag{8}$$

Hence, the result for the straight TE is recovered.
The formula of Howe for the case of saw-tooth shaped TE serrations (5) is

$$\hat{S}(\omega) = \frac{2L}{\pi R^2} \frac{1}{c_0} \sum_{n=-\infty}^{\infty} \frac{\left(\frac{\omega h}{U_c} \right)^2 + (k_n h)^2}{\left(4 \left(\frac{\omega h}{U_c} \right)^2 - n^2 \pi^2 \right)^2} \left(1 - \frac{\cos\left(2 \frac{\omega h}{U_c} \right)}{\cos(n\pi)} \right) \Phi_p \left(\frac{\omega}{U_c}, k_n \right). \tag{9}$$

Again, the original expression by Howe was multiplied by a factor of 2. Due to symmetry eq. 9 can be expressed as

$$\hat{S}(\omega) = \hat{S}_0(\omega) + 2\hat{S}_{n+}(\omega) \tag{10}$$

with

$$\hat{S}_0(\omega) = \frac{2L}{\pi R^2}\frac{1}{c_0}\frac{1}{16\left(\frac{\omega h}{U_c}\right)^2}\left(1-\cos\left(2\frac{\omega h}{U_c}\right)\right)\Phi_p\left(\frac{\omega}{U_c},0\right) \tag{11}$$

and

$$\hat{S}_{n+}(\omega) = \frac{2L}{\pi R^2}\frac{1}{c_0}\sum_{n=1}^{\infty}\frac{\left(\frac{\omega h}{U_c}\right)^2+(k_n h)^2}{\left(4\left(\frac{\omega h}{U_c}\right)^2-n^2\pi^2\right)^2}\left(1-\frac{\cos\left(2\frac{\omega h}{U_c}\right)}{\cos(n\pi)}\right)\Phi_p\left(\frac{\omega}{U_c},k_n\right). \tag{12}$$

By expanding the cosine terms of eq. 11 and eq. 12 with a Taylor series, we find the limits divided by the formula for the straight TE (eq. 4) for $\lambda \to \infty$ and $h \to 0$

$$\lim_{\lambda\to\infty,h\to 0}\frac{\hat{S}_0(\omega)}{S(\omega)} = \lim_{\lambda\to\infty,h\to 0}\left(1-\frac{2}{3}\left(\frac{\omega h}{U_c}\right)^2+\mathcal{O}\left(\frac{\omega h}{U_c}\right)^4\right) = 1 \tag{13}$$

and

$$\lim_{\lambda\to\infty,h\to 0}\frac{\hat{S}_{n+}(\omega)}{S(\omega)} = 0. \tag{14}$$

The expression for the straight TE is recovered and the introduction of the factor 2 is justified.

4. RESULTS

4.1 Aerofoil polar and mean surface pressure

The lift and drag polar of the DTU-LN18 aerofoil at Reynolds number $Re = 1.6 \cdot 10^6$ is shown in figure 3. The measurements are compared to 2 dimensional CFD computations with the Ellipsys2D code (12, 13, 14).

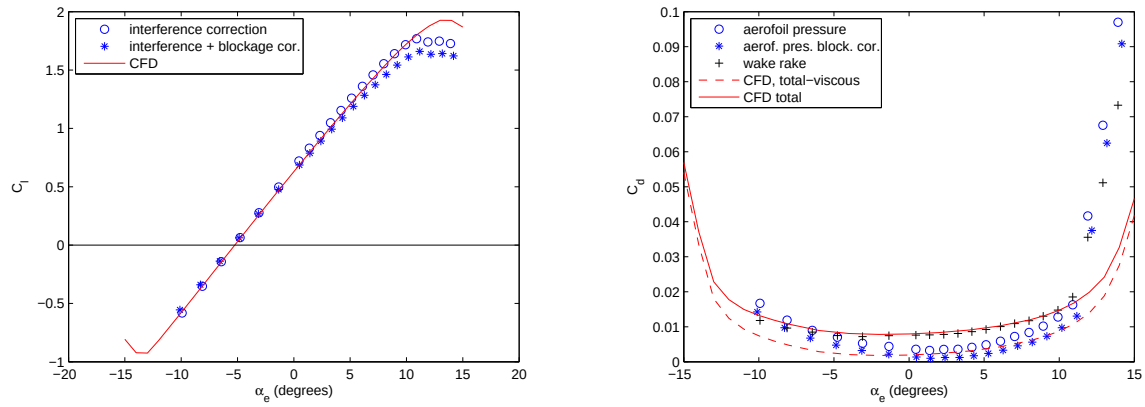

(a) C_l vs α_e (b) C_d vs α_e

Figure 3 – Polar of the DTU-LN118 aerofoil at Reynolds number $Re = 1.6 \cdot 10^6$.

The measured and computed lift curves are in excellent agreement in the linear range of the polar (approximately $-10° < \alpha_e < 10°$). The maximum lift angle and the maximum lift of the measured curve are lower than for the curve computed with CFD. At the high AoAs the flow is three dimensional. The computational set-up is two dimensional. The wind tunnel corrections are derived based on two dimensional considerations. Especially vortices developing at the junction of the aerofoil and the wind tunnel wall can significantly change the stall behaviour. Hence, both computation and measurement are uncertain in the range of high angles of attack.

The drag coefficient, figure 3(b), was measured by means of the pressure deficit in the wake and by means of aerofoil surface pressures. The wake rake measurement captures the viscous and the pressure contribution of the drag and compares very well to the computation of the total drag within the linear range of the polar.

The aerofoil pressure drag does not include the viscous part of the drag. It corresponds to the computations in which the viscous part was subtracted. A good agreement between between measurement and computation is only achieved in a limited range of AoAs ($0^\circ < \alpha_e < 6^\circ$). The drag coefficient is very sensitive to AoA changes. The uncertainty in determining the zero geometric AoA might be responsible for the difference. The range of AoAs with low drag is narrower in the measurement, because stall occurs at lower AoAs.
The measured pressure distributions on the suction side of the aerofoil are in very good agreement with the CFD computations, figure 4. The typical hump at the location of transition is captured well by the computation.

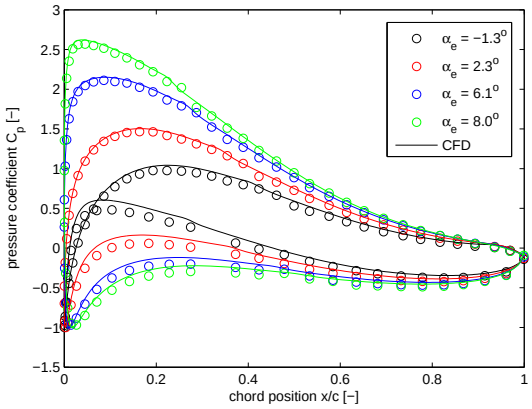

Figure 4 – Pressure distributions at Reynolds number $Re = 1.6 \cdot 10^6$.

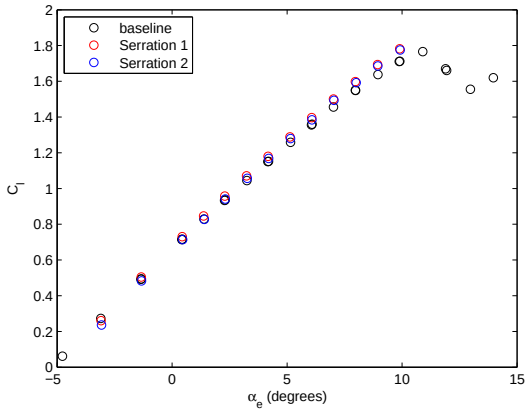

Figure 5 – Aerofoil lift curve for baseline and serrated TE.

Hence, there is a very low uncertainty introduced when the boundary layer parameters obtained by CFD computations are used as input to the noise model (provided that only AoAs in the linear range of the polar are considered).
Figure 5 shows the lift curve at Reynolds number $Re = 1.6 \cdot 10^6$ for the baseline aerofoil and the configurations with the two different serrations attached. The aerodynamic performance of the aerofoil is hardly influenced by the serrations. First at AoAs $\alpha_e > 6^\circ$ the flap effect of the serrations can be noticed by a very small increase of the lift coefficient. However, it has to be noted that the pressure distribution on the serrations was not measured.

4.2 Far field sound measurements

The far field sound measurements of the aerofoil with the straight TE and the two types of serrations are shown in figure 6 for 4 characteristic AoAs. The three first AoAs are in the linear range of the aerofoil polar. The highest AoA ($\alpha_e = 9.9^\circ$) is at the maximum lift of the aerofoil polar. In all cases the difference between the noise levels of the two serration types is less than 0.8 dB. Serration 2 gives a marginally higher reduction. For an AoA of $\alpha_e = -1.3^\circ$ the serrations reduce the noise level only in the frequency range above 1600 Hz. The noise reduction due to the serrations is increased as the frequency goes up (i.e. less than 1dB at 1600 Hz while at least 5 dB above 3000 Hz). In the frequency range below 1500 Hz the far field noise level of the aerofoil with serrated TE is nearly constant for the three AoAs in the linear range of the polar. The serrations cannot reduce the noise emission below this threshold value. Unlike the $\alpha_e = -1.3^\circ$ case, results for higher AoAs show very good noise reduction at low frequencies (below 1600 Hz). It has also to be noted that the noise generated by the baseline aerofoil has significantly increased in this frequency range compared to the case with AoA $\alpha_e = -1.3^\circ$. The result for $\alpha_e = 2.3^\circ$ shows reduction over the whole frequency range from about 3dB at low frequency to over 5 dB at higher frequencies. For $\alpha_e = 6.1^\circ$ noise is reduced in the low frequency range. For frequency higher than approx. 1400 Hz there is almost no reduction compared to the baseline. There could be some cross flow from pressure to suction side through the serrations which causes vortex shedding from the serrations. The vortex shedding is an additional noise source which counteracts the noise reduction. The noise levels in both serrated configurations are louder than the baseline when the aerofoil is stalled ($\alpha_e = 9.9^\circ$), in particular above 1000 Hz.

4.3 Noise modelling

Computations with the improved TNO model (3) were compared to measurements of the far field TE noise emitted of the baseline aerofoil with straight TE, figure 7. In figure 7(a) the contribution of suction and pressure side were taken into account in the model. In figure 7(b) only the contribution from the suction side was taken into account. For frequencies lower than 2000 Hz the prediction of the far field sound concurs with the measurements. However, the slope of the predicted spectra is flatter than the one of the measured spectra and

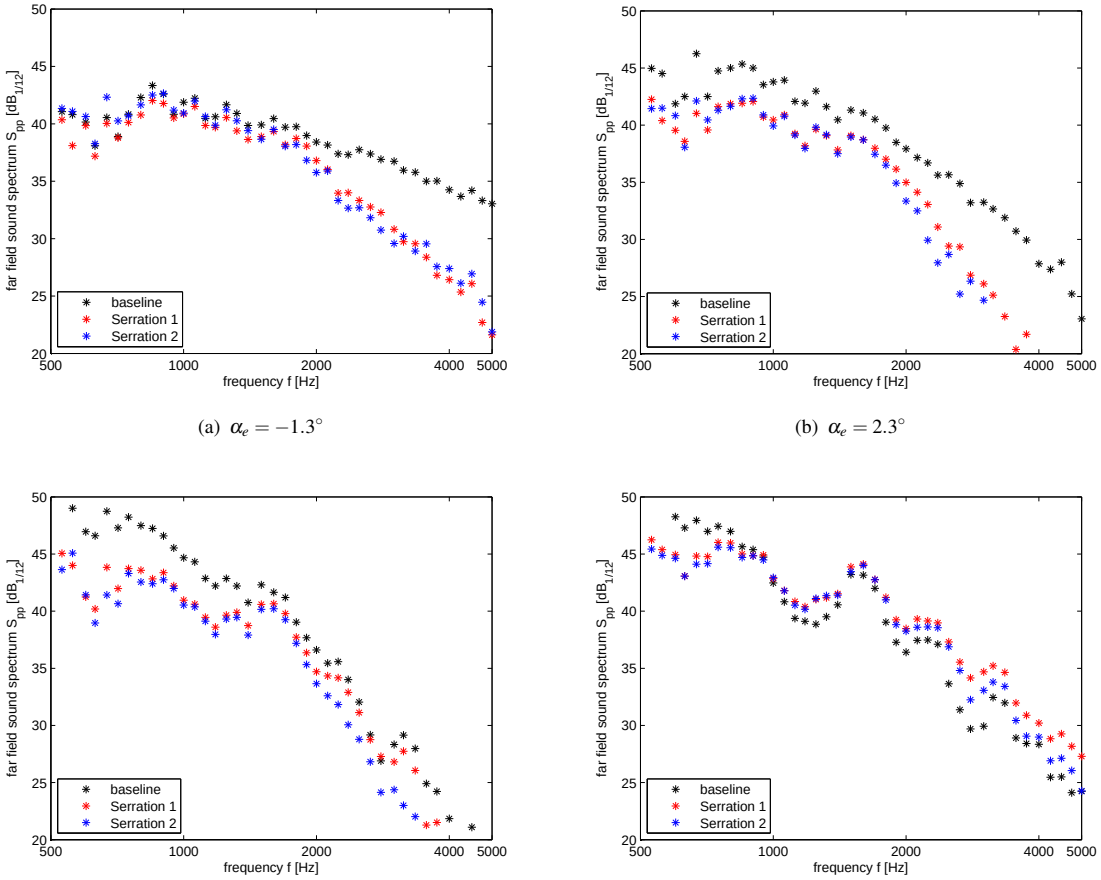

(a) $\alpha_e = -1.3^\circ$ (b) $\alpha_e = 2.3^\circ$

(c) $\alpha_e = 6.1^\circ$ (d) $\alpha_e = 9.9^\circ$

Figure 6 – Far field sound measurements at Reynolds number $Re = 1.6 \cdot 10^6$.

the sound pressure level is predicted too high for frequencies above 2000 Hz. For the AoAs $\alpha_e = -1.3^\circ$ and $\alpha_e = 2.3^\circ$ the peak noise radiating frequency of the computed spectra is higher than the one of the measured spectra. For the AoAs $\alpha_e = 6.1^\circ$ and $\alpha_e = 9.9^\circ$ the peak noise radiating frequency is predicted well, but the pressure side contribution to the emitted far field sound creates an inflection point at a frequency of about 2000 Hz. The inflection is not seen in the measured spectra and the computed spectra fit better to the measured ones if only the suction side contribution is taken into account. In literature (15, 16, 17, 18, 3) there is a consensus that the contribution from both sides should be taken into account.

The case with AoA $\alpha_e = 2.3^\circ$ was chosen to test the models for serrated TEs, figure 8, because the measurements showed that the serrations worked best for this angle and the computations gave good results for the straight TE case when using the standard approach (adding suction and pressure side contribution). The results are shown for Serration 1 and the wave length of the serrations λ and half of the peak-to-peak amplitude of the serrations h were set according to the geometry of Serration 1. The noise reduction predicted by both theoretical models is more than 15 dB larger than the noise reduction obtained in the experiment. The saw-tooth model gives an larger reduction than the sinusoidal model. The assumptions made to derive those analytical models are too simple to describe the complex flow interaction at the serrated TE. Three phenomena were identified which can possibly counteract the noise reduction by the serrations. In the case of a serrated TE the flow does not leave the aerofoil in the main stream direction. It tends to turn at the serration and leave the edge in an angle which is larger than if it was still following the mean stream direction. Hence, the radiation of sound increases. This phenomenon can to some extend be simulated by increasing the wave length of the serrations λ in the model to a larger value than the actual geometric wave length. Second, when the flow turns at the serrated TE it will roll up and form vortices. Those vortices act as additional sound sources. They are not described in the model. Third, in most flow conditions there will be cross flow from the pressure to the suction side through the serrations. This also leads to vortex shedding and an increase of the emitted sound.

The sensitivity of the saw-tooth model (9(a)) and the sinusoidal model (9(b)) for changes of the wave length of the serrations λ is investigated. Both models are very sensitive to changes of the wave length λ. A doubling

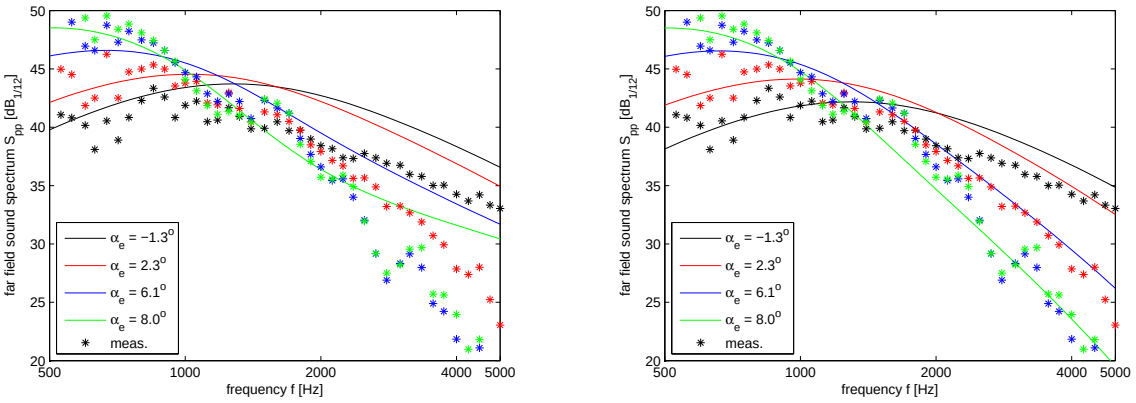

(a) suction and pressure side contribution (b) suction side contribution

Figure 7 – Far field sound pressure spectra of the baseline DTU-LN118 aerofoil at Reynolds number $Re = 1.6 \cdot 10^6$. lines: computations, stars: measurements.

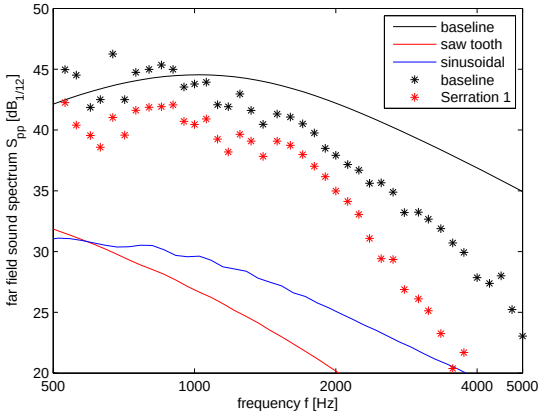

Figure 8 – Far field sound pressure spectra of the baseline and serrated configurations at Reynolds number $Re = 1.6 \cdot 10^6$ and angle of attack $\alpha_e = 2.3°$. lines: computations, stars: measurements.

causes changes of the sound pressure level between 3 and 5 dB. The sound pressure level changes are not a linear function of the wave length λ. The model for a sinusoidally shaped serrated TE can reproduce the level of the sound pressure spectra in the frequency range between 500 Hz and 2000 Hz if the wave length is 8 times the geometrical wave length, but the spectral shape is not correct. The saw-tooth serration model yields even for $\lambda = 8 \cdot \lambda_e$ higher reductions of the sound pressure level than the measurement. The spectral shape does fit either.

5. CONCLUSIONS

The aerodynamic and acoustic performance of two different geometries of saw-tooth trailing edge serrations were tested in the aero-acoustic wind tunnel of Virginia Tech university. An aerofoil developed for the outer sections of wind turbine blades was used as baseline.

The aerodynamic data corrected for wind tunnel effects fitted well to CFD computations. The measurements showed that the influence of the serrations on the lift curve was negligible, a desired result. For very high angles of attack the lift was marginally increased due to the flap effect of the serrations, i.e. approx. 3.5% increase of the lift coefficient for an angle of attack of 10° (close to stall). The emitted far field trailing edge noise was reduced effectively by the two types of serrations for angles of attack in the linear range of the polar. They were most effective for low angles of attack in the high frequency range, up to 8 dB. For higher angles of attack in the linear range of the polar the noise reduction increased for low frequencies, but the absolute reduction of the noise level was smaller (3 to 5 dB). When the aerofoil was in stall, the emitted far field sound was higher for the serrated cases. Both serration geometries yielded similar noise levels for all angels of attack, within 0.8 dB difference.

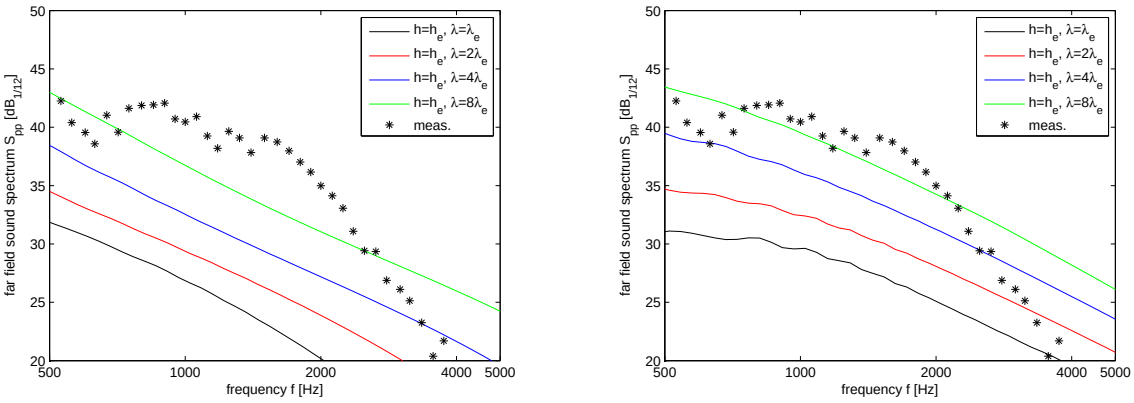

(a) Saw-tooth model

(b) Sinusoidal model

Figure 9 – Far field sound pressure spectra of the aerofoil with Serration 1 at Reynolds number $Re = 1.6 \cdot 10^6$ and angle of attack $\alpha_e = 2.3°$. lines: computations, stars: measurements; h_e, λ_e: geometric values of Serration 1.

Computations with the improved TNO model (3) were performed and compared to the far field sound measurements. The level of the measured and computed far field sound pressure in the low frequency range as well as the peak radiating frequency fitted well. But the slope of the computed spectra was flatter in the high frequency range. The analytical models for the sound emitted from a serrated trailing edge by Howe (4, 5) were coupled to the improved TNO model and compared to measurement. A factor of 2 was introduced to both expressions in order make them converge to the result for a straight trailing edge in the limit of vanishing serration amplitude and infinitely long wave length. They yielded much higher noise reductions compared to the straight edge case than it was observed in the measurements. The main shortcoming of the models might be the relatively crude assumptions about the flow at the trailing edge. In order to improve the model the complex flow conditions at the serrated trailing edge have to be investigated in more detail. 3 dimensional CFD computations and PIV experiments are suitable for this purpose.

ACKNOWLEDGEMENTS

The wind tunnel test was founded by the Energy Technology Development and Demonstration Program (EUDP-2011-I, J. nr. 64011-0094) under the Danish Energy Agency. Parts of the presented work were carried out in the project WINDTRUST: 'Demonstration of more reliable innovative designs on a 2MW Wind turbine' under grant agreement no. 322449 of EU's Seventh Framework Programme for Research (FP7). The authors want to acknowledge Patricio Ravetta from AVEC, Inc. for performing the microphone array measurements and providing the post processed data.

REFERENCES

1. Oerlemans S, Fisher M, Maeder T, Kögler K. Reduction of Wind Turbine Noise Using Optimized Airfoils and Trailing-Edge Serrations. AIAA Journal. 2009;47(6):1470–1481.

2. Fink MR, Bailey DA. Model Tests of Airframe Noise Reduction Concepts. In: Proceedings. AIAA Paper 80-0979; 1980. .

3. Bertagnolio F, Fischer A, Zhu WJ. Tuning of turbulent boundary layer anisotropy for improved surface pressure and trailing-edge noise modeling. J Sound Vib. 2014;333:991–1010.

4. Howe MS. Aerodynamic Noise of a Serrated Trailing Edge. J of Fluids and Structures. 1991;5:33–45.

5. Howe MS. Noise produced by a sawtooth trailing edge. J Acoust Soc Am. 1991;90(1):482–487.

6. Devenport WJ, Burdisso RA, Borgoltz A, Ravetta P, Barone MF, Brown KA, et al. The Kevlar-walled anechoic wind tunnel. J Sound Vib. 2013;332:3971–3991.

7. Mueller TJ. Aeroacoustic Measurements. Springer; 2002.

8. Cheng J, Zhu WJ, Fischer A, Garcia NR, Madsen J, Chen J, et al. Design and validation of the high performance and low noise CQU-DTU-LN1 airfoils. Wind Energ. 2013 August;DOI:10.1002/we.

9. Howe MS. A Review of the Theory of Trailing Edge Noise. J Sound Vib. 1978;61(3):437–465.

10. Amiet RK. Noise due to Turbulent Flow Past a Trailing Edge. J Sound Vib. 1976;47(3):387–393.

11. Parchen R. Progress report DRAW: A Prediction Scheme for Trailing-Edge Noise Based on Detailed Boundary-Layer Characteristics. TNO Institute of Applied Physics, The Netherlands; 1998.

12. Sørensen NN. General Purpose Flow Solver Applied to Flow over Hills. Risø National Laboratory, Roskilde, Denmark; 1995.

13. Michelsen JA. Basis3D - A Platform for Development of Multiblock PDE Solvers. Technical University of Denmark; 1992.

14. Michelsen JA. Block Structured Multigrid Solution of 2D and 3D Elliptic PDE's. Technical University of Denmark; 1994.

15. Brooks TF, Hodgson TH. Trailing Edge Noise Prediction from Measured Surface Pressures. J Sound Vib. 1981;78(1):69–117.

16. Brooks TF, Pope SD, Marcolini MA. Airfoil Self-Noise and Prediction. Langley Research Center; 1989.

17. Moriarty P, Guidati G, Migliore P. Prediction of Turbulent Inflow and Trailing-Edge Noise for Wind Turbines. In: Proc. of the 11^{th} AIAA/CEAS Aeroacoustics Conf. AIAA Paper 2005-2881. Monterey, CA; 2005. .

18. Kamruzzaman M, Lutz T, Herrig A, Krämer E. Semi-empirical Modeling of Turbulent Anisotropy for Airfoil Self Noise Predictions. AIAA Journal. 2012;50(1):46–60.